Supporting Information

Rational design of single-atom catalysts for efficient H_2O_2 production via a four-step strategy

Shu-Long Li [a,b,c], *Xiaogui Song*[a], *Zuhui Zhou*[a], *Hongyuan Zhou*[a], *Liang Qiao*[b]*, *Yong Zhao*[a,d]*, *and Li-Yong Gan*[e]*

[a] Institute for Advanced Study, Chengdu University, Chengdu 610106, China

[b] School of Physics, University of Electronic Science and Technology of China, Chengdu 611700, China

[c] Western Superconducting Technologies Co, Ltd., Xi`an 710018, China

[d] College of Physics and Energy, Fujian Normal University, Fuzhou 350117, China

[e] College of Physics and Center of Quantum Materials and Devices, Chongqing University, Chongqing 401331, China

*E-mail: liang.qiao@uestc.edu.cn (L. Q.), zhaoyong@cdu.edu.cn (Y. Z.), and ganly@cqu.edu.cn (L.-Y. G.)

Gibbs Free Energy Computations

The electrochemical ORR reactions can be divided into $2e^-$ ORR and $4e^-$ ORR [1]. For the $4e^-$ ORR reaction, the reaction intermediates include OOH*, O*, and OH*, and the product is H_2O [2]. For the $2e^-$ ORR reactions, the only reaction intermediate is OOH* and the product is H_2O_2 [3]. The ΔG of intermediates OOH*, O*, and OH* were calculated as follows:

$$\Delta G_{OOH} = G_{OOH} - G_* - (2G_{H_2O} - 3/2G_{H_2}) \quad (1)$$

$$\Delta G_O = G_O - G_* - (G_{H_2O} - G_{H_2}) \quad (2)$$

$$\Delta G_{OH} = G_{OH} - G_* - (G_{H_2O} - 1/2G_{H_2}) \quad (3)$$

$$G_{O_2}(g) = 2G_{H_2O}(l) - 2G_{H_2} + 4 \times 1.23 \quad (4)$$

where * denotes the adsorption carrier of TM-GY. where G_* represents the total energy of the TM-GY, and G_{OOH}, G_O and G_{OH} denote the total energies when the intermediates OOH*, O*, and OH* are adsorbed on TM-GY, respectively. Due to inaccuracies in DFT calculations for gaseous O_2 in the high spin ground state, $G_{O_2}(g)$ was calculated using Eq. (4), assuming equilibrium between gas-phase and liquid-phase water at room temperature reached equilibrium [4].

The $2e^-$ ORR reaction process:

$$* + OO + H_2O + e^- \rightleftharpoons OOH^* \quad (5)$$

$$OOH^* + H_2O + e^- \rightleftharpoons H_2O_2 + OH^- \quad (6)$$

The $4e^-$ ORR reaction process:

$$* + OO + H_2O + e^- \rightleftharpoons OOH^* + OH^- \quad (7)$$

$$OOH^* + H_2O + e^- \rightleftharpoons O^* + H_2O + OH^- \quad (8)$$

$$O^* + H_2O + e^- \rightleftharpoons OH^* + OH^- \quad (9)$$

$$OH^* + H_2O + e^- \rightleftharpoons H_2O + OH^- \quad (10)$$

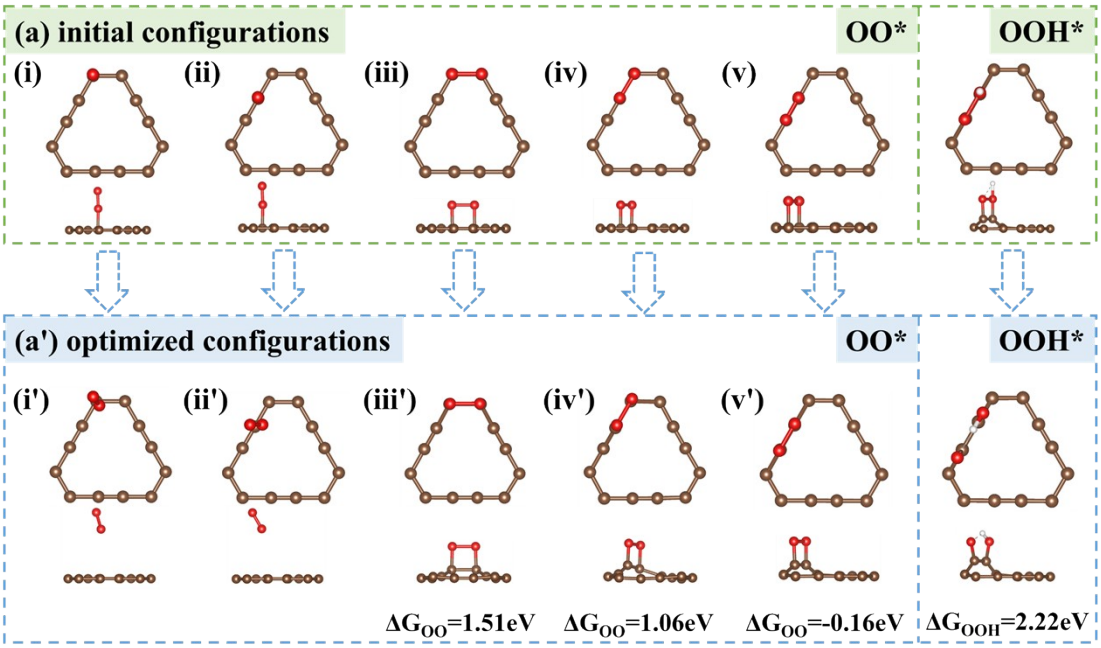

Fig. S1. The H_2O_2 performance of primitive GY.

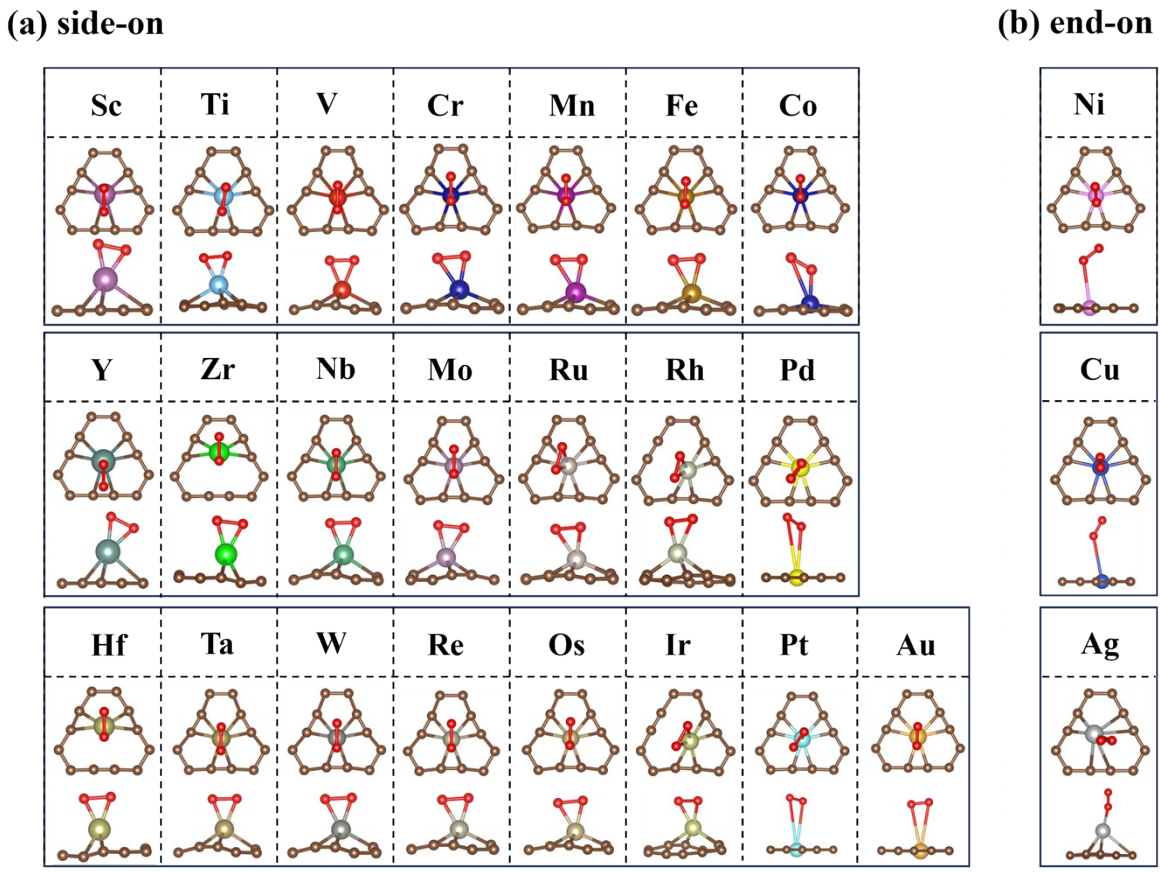

Fig. S2. The side-on and end-on O_2 adsorption configurations on TM-GY.

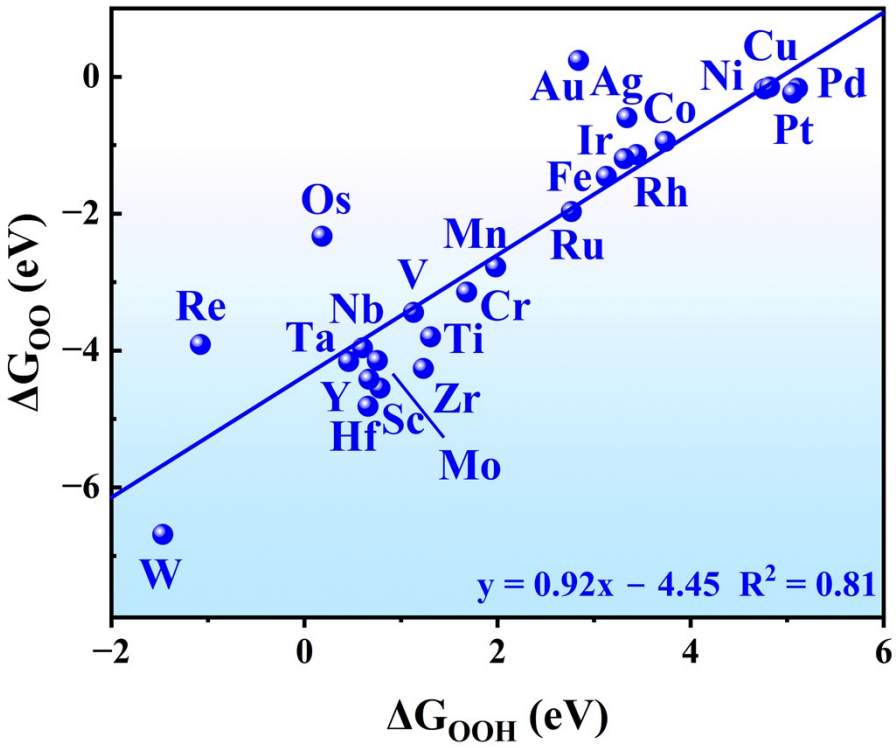

Fig. S3. The relationship between ΔG_{OOH} and ΔG_{OO}.

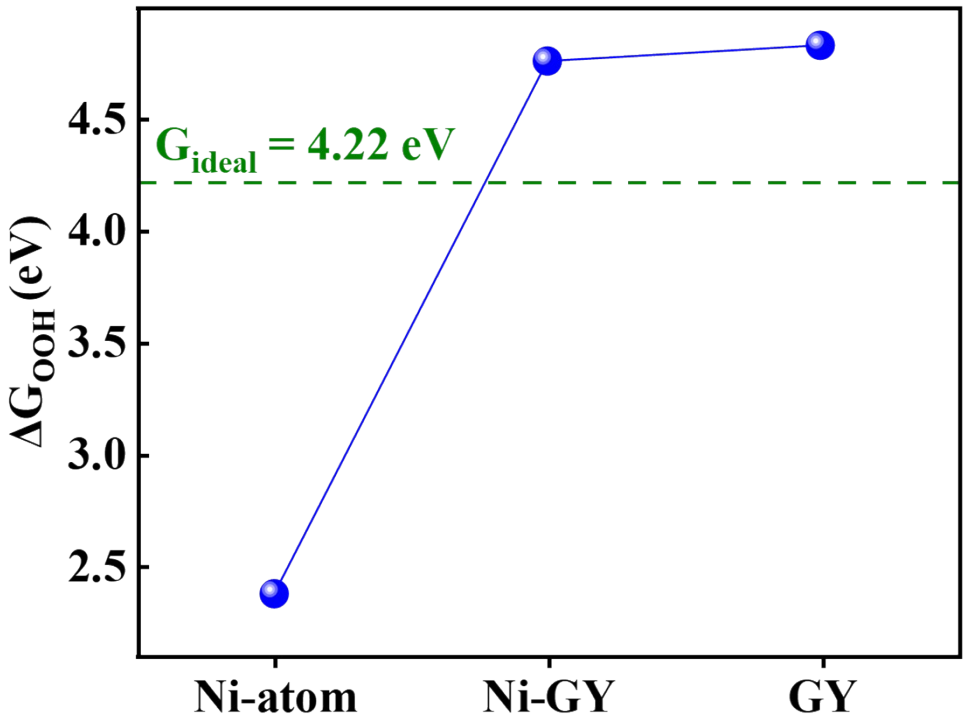

Fig. S4. Comparison of ΔG_{OOH} of Ni-atom, Ni-GY, GY.

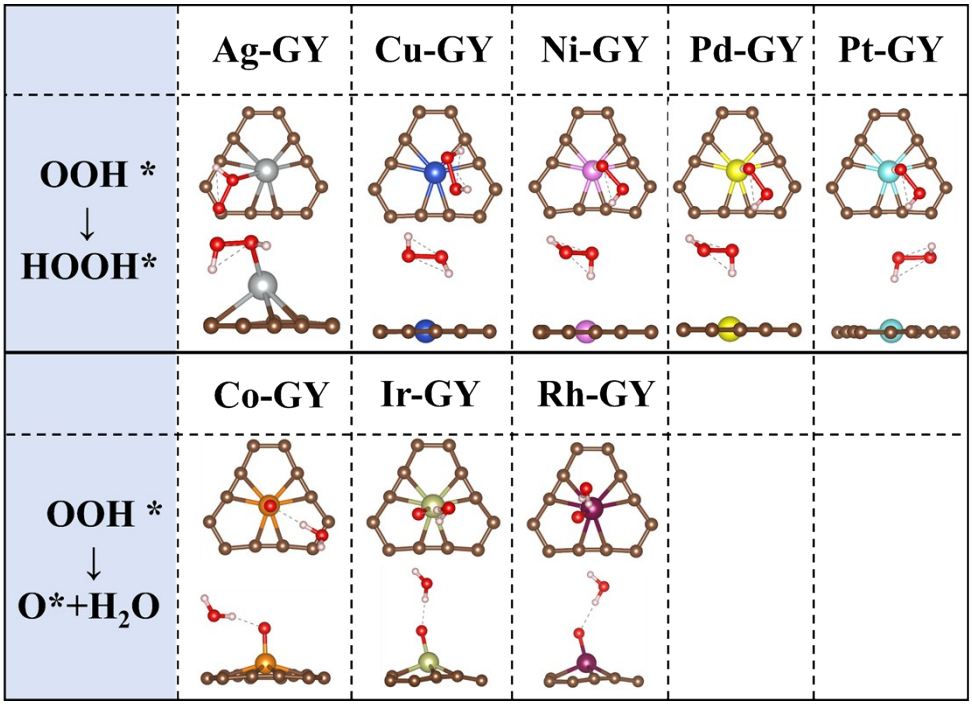

Fig. S5. the configuration of TM-GY after the OOH* hydrogenation to form H_2O_2.

Table S1. The d-orbital (θ_d), atomic electronegativity (E_M) and atom-radius (R).

TM	θ_d	E_M	R		TM	θ_d	E_M	R		TM	θ_d	E_M	R
Sc	1	1.36	1.64		Y	1	1.22	1.80		Hf	2	1.32	1.59
Ti	2	1.54	1.45		Zr	2	1.33	1.60		Ta	3	1.51	1.48
V	3	1.63	1.35		Nb	4	1.59	1.48		W	4	2.36	1.41
Cr	5	1.66	1.27		Mo	5	2.16	1.40		Re	5	1.93	1.46
Mn	5	1.55	1.32		Ru	7	2.20	1.32		Os	6	2.18	1.34
Fe	6	1.83	1.27		Rh	8	2.28	1.34		Ir	7	2.20	1.36
Co	7	1.88	1.26		Pd	10	2.20	1.37		Pt	9	2.28	1.39
Ni	8	1.92	1.24		Ag	10	1.93	1.44		Au	10	2.54	1.44
Cu	10	1.90	1.28										

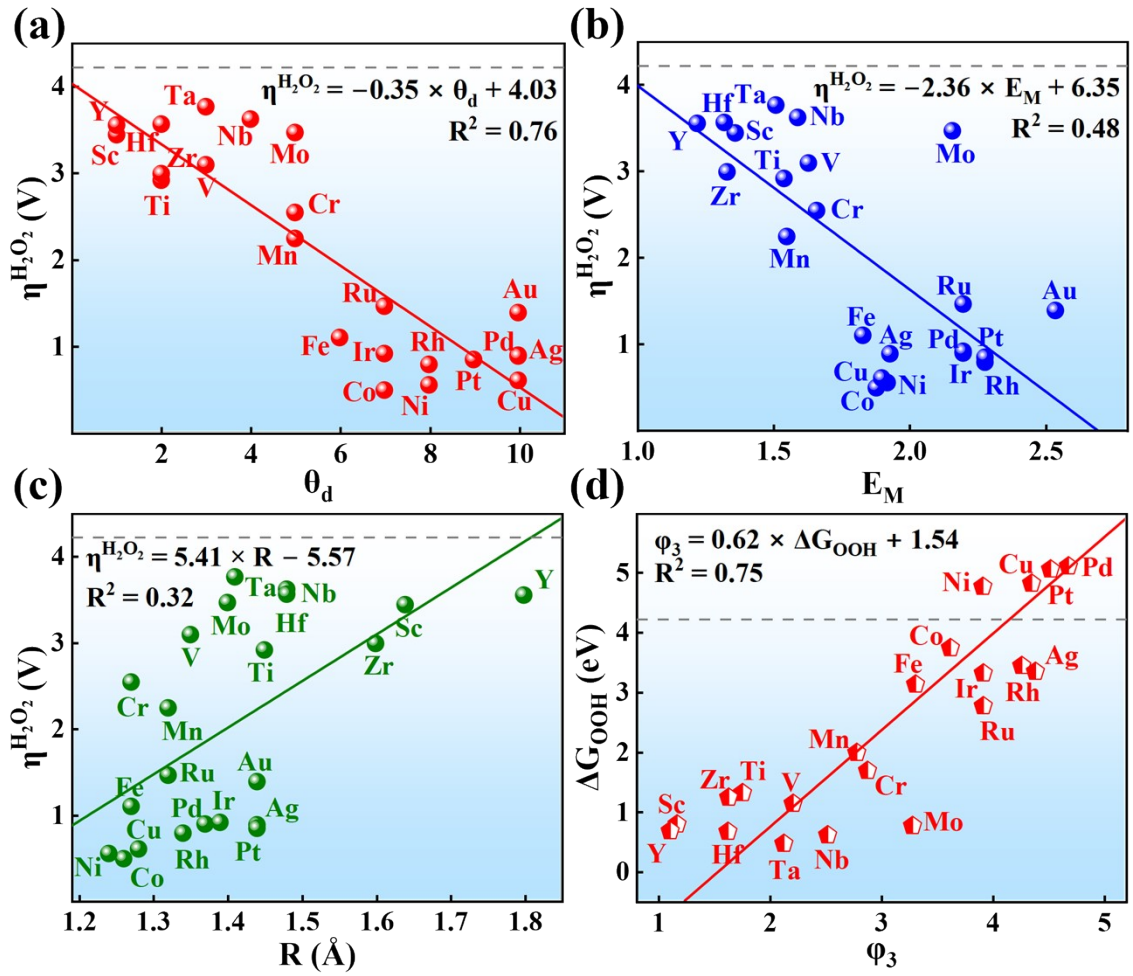

Fig. S6. The scaling relationship between η^{H2O2} and d electrons(θ_d) (a), the electronegativity (E_M) (b), and the atomic radius (R) (c). (d)The scaling relationship between ΔG_{OOH} and φ_3 for TM-GY.

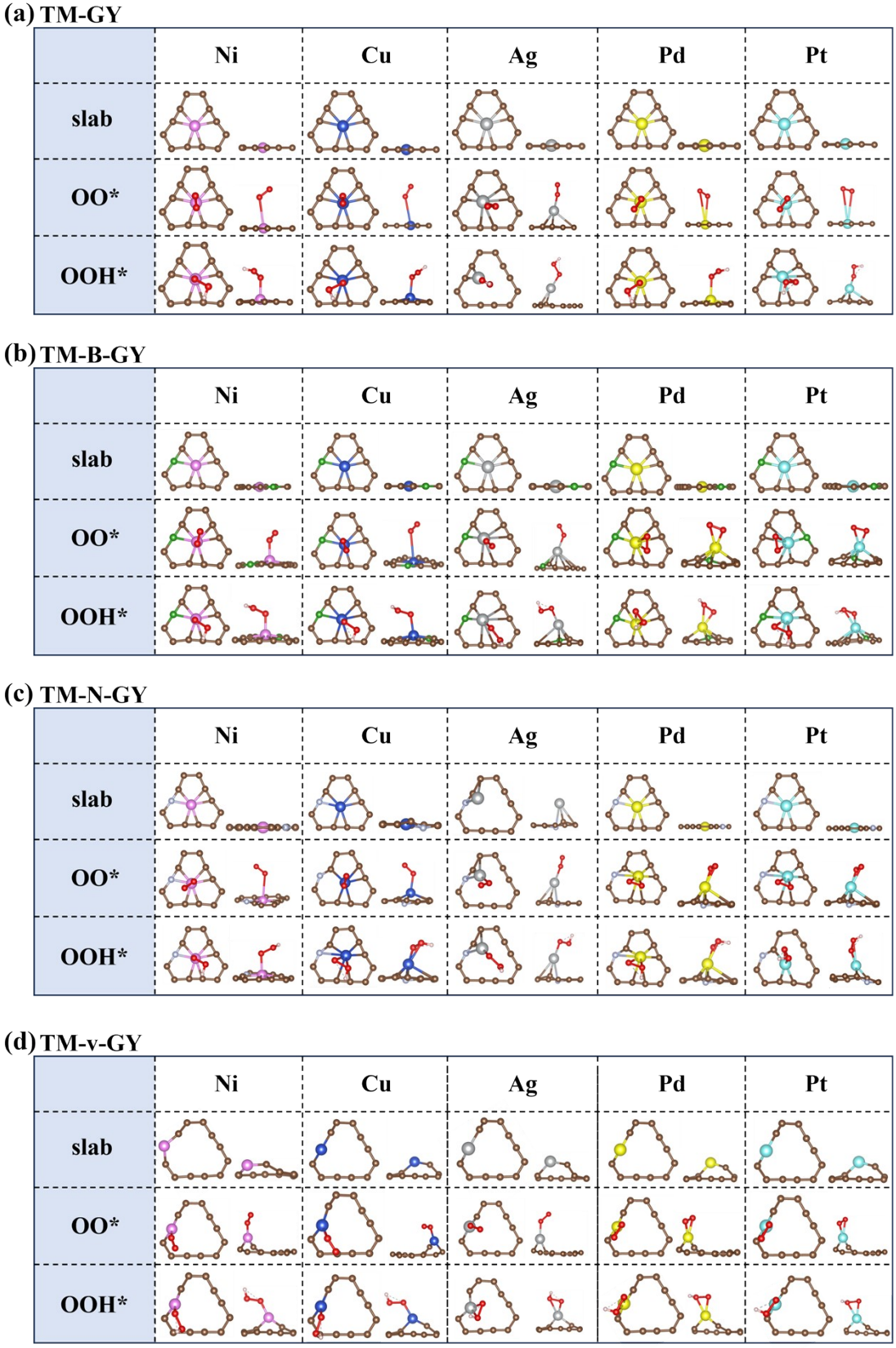

Fig. S7. The configuration of OO* and OOH* for TM-GY, TM-B-GY, TM-N-GY, and TM-v-GY.

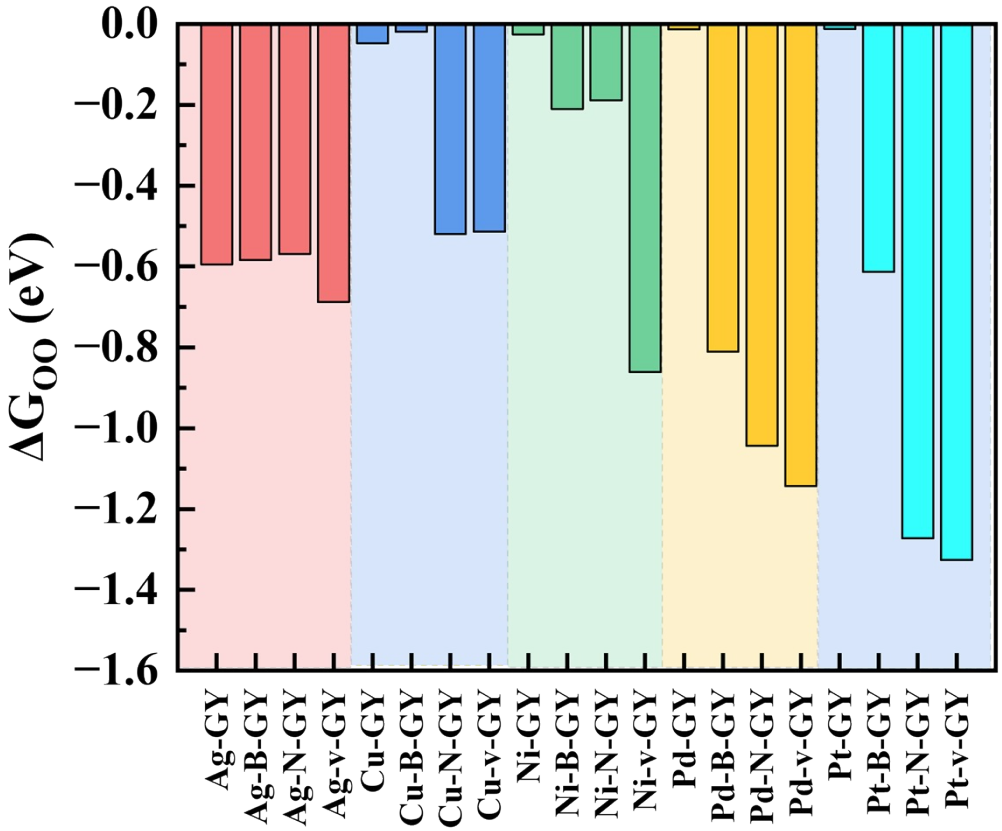

Fig. S8. The ΔG_{OO} for TM-NM-GY (TM = Ag, Cu, Ni, Pd and Pt; NM = B, N doping or C vacancy).

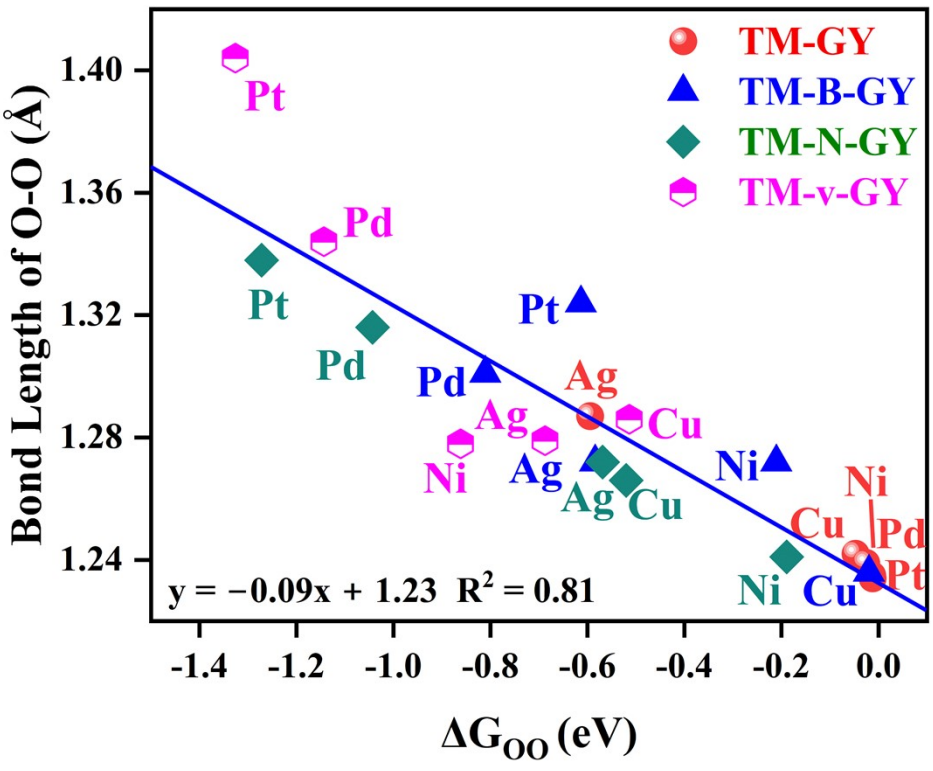

Fig. S9. The relationship between the ΔG_{OO} and the O-O bond length on TM-NM-GY.

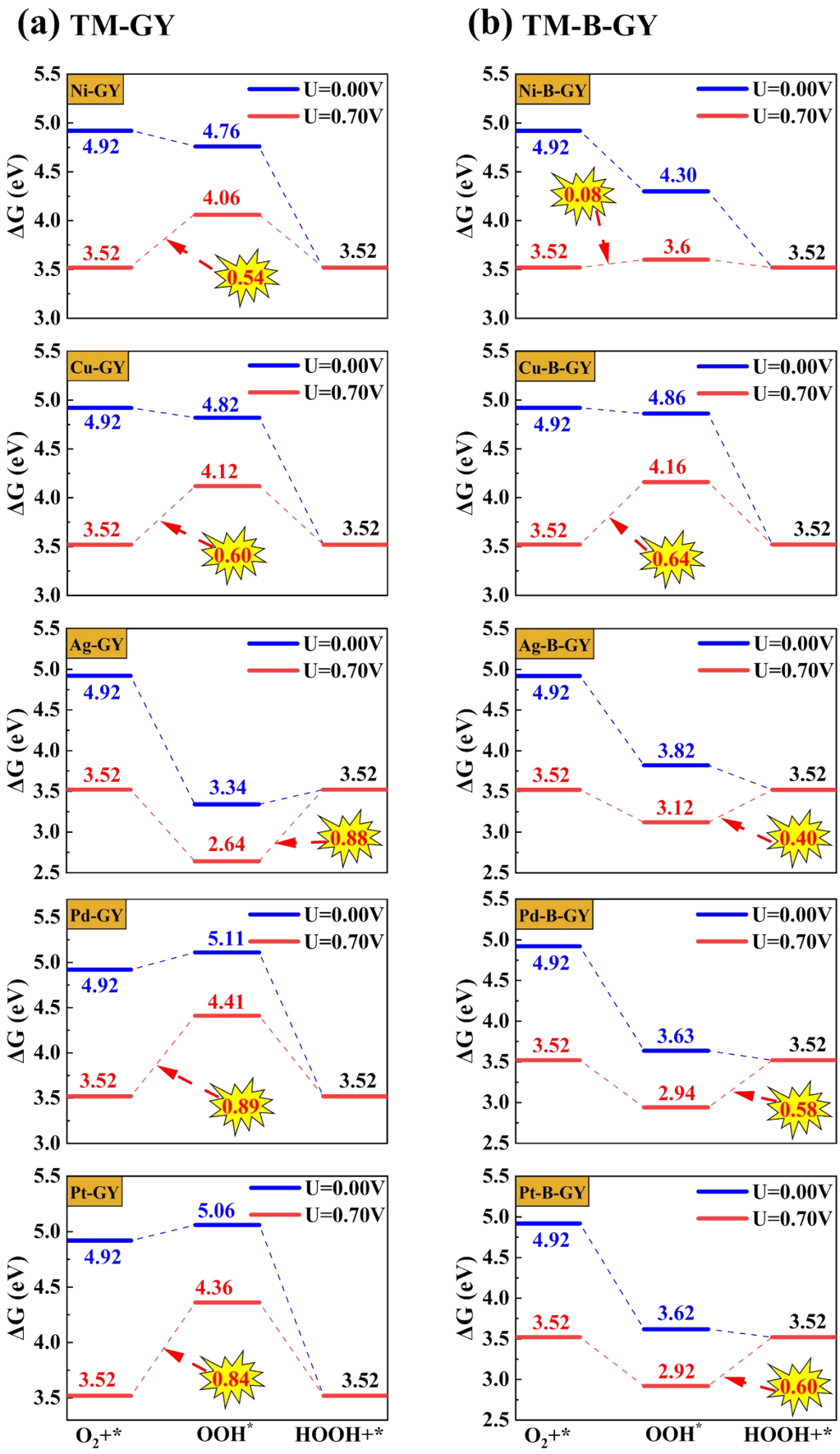
(a) TM-GY
(b) TM-B-GY
Ni-GY
Cu-GY
Ag-GY
Pd-GY
Pt-GY
Ni-B-GY
Cu-B-GY
Ag-B-GY
Pd-B-GY
Pt-B-GY
U=0.00V
U=0.70V
ΔG (eV)
4.92
4.76
4.06
3.52
0.54
4.82
4.12
0.60
3.34
2.64
0.88
5.11
4.41
0.89
5.06
4.36
0.84
4.30
0.08
3.6
4.86
4.16
0.64
3.82
3.12
0.40
3.63
2.94
0.58
3.62
2.92
0.60
O2+*
OOH*
HOOH+*

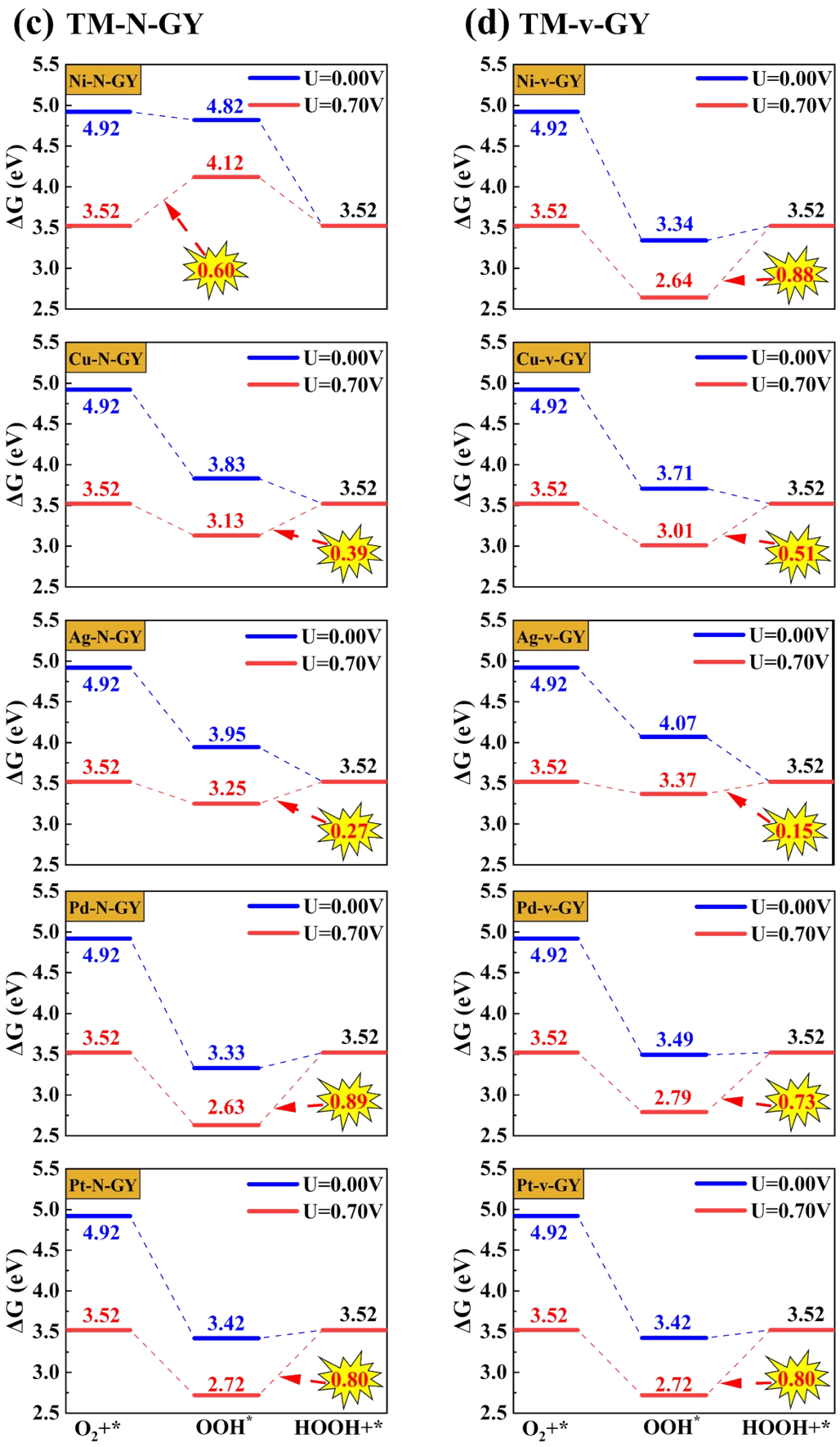

Fig. S10. The Free energy diagrams of $2e^-$ ORR for H_2O_2 product on TM-NM-GY.

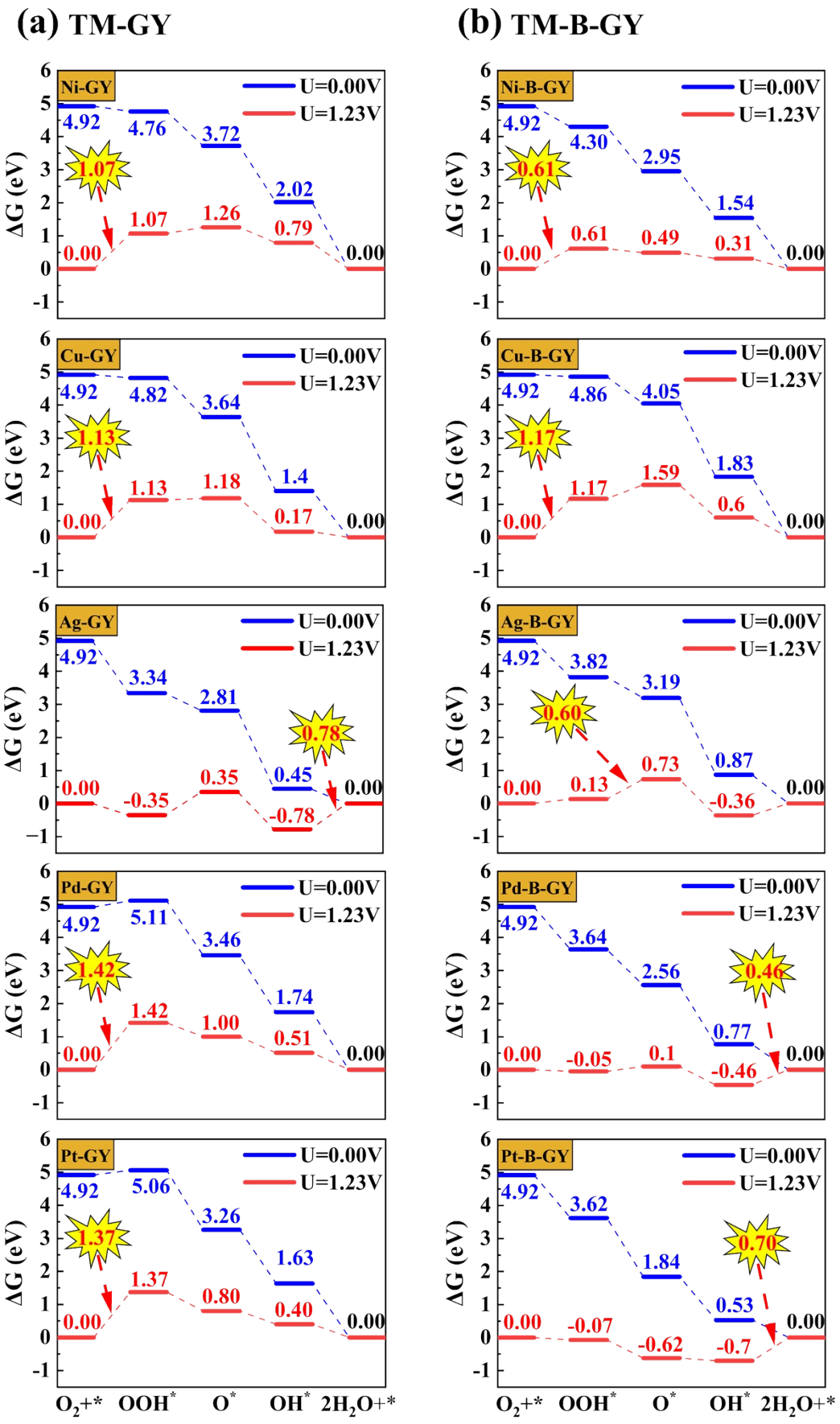
(a) TM-GY
(b) TM-B-GY
Ni-GY
Cu-GY
Ag-GY
Pd-GY
Pt-GY
Ni-B-GY
Cu-B-GY
Ag-B-GY
Pd-B-GY
Pt-B-GY
U=0.00V
U=1.23V
ΔG (eV)
4.92 4.76 3.72 2.02 0.00
1.07 1.07 1.26 0.79 0.00
4.92 4.82 3.64 1.4 0.00
1.13 1.13 1.18 0.17 0.00
4.92 3.34 2.81 0.45 0.00
0.78 0.00 -0.35 0.35 -0.78 0.00
4.92 5.11 3.46 1.74 0.00
1.42 0.00 1.42 1.00 0.51 0.00
4.92 5.06 3.26 1.63 0.00
1.37 0.00 1.37 0.80 0.40 0.00
4.92 4.30 2.95 1.54 0.00
0.61 0.00 0.61 0.49 0.31 0.00
4.92 4.86 4.05 1.83 0.00
1.17 0.00 1.17 1.59 0.6 0.00
4.92 3.82 3.19 0.87 0.00
0.60 0.00 0.13 0.73 -0.36 0.00
4.92 3.64 2.56 0.77 0.00
0.46 0.00 -0.05 0.1 -0.46 0.00
4.92 3.62 1.84 0.53 0.00
0.70 0.00 -0.07 -0.62 -0.7 0.00
O2+* OOH* O* OH* 2H2O+*

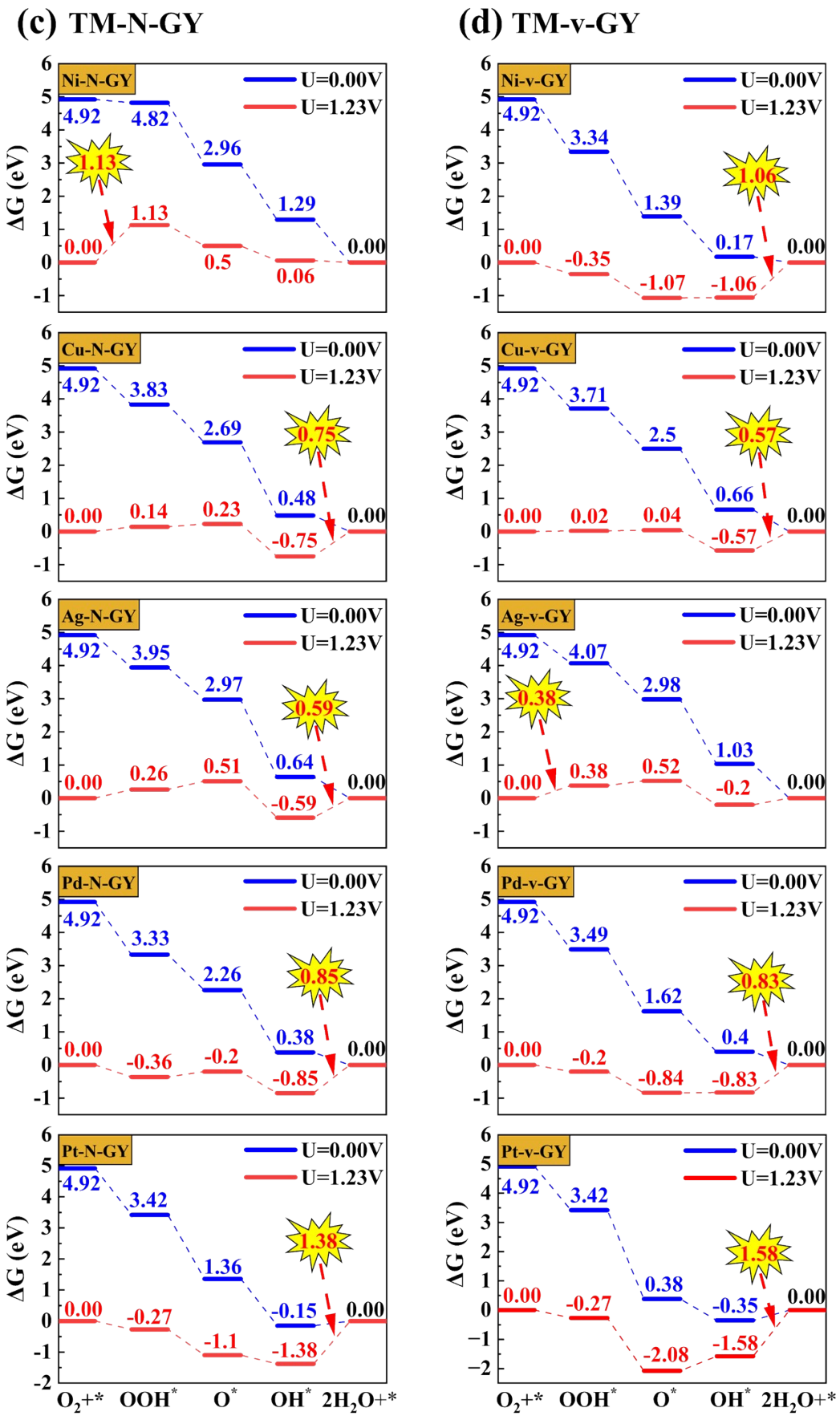

Fig. S11. The Free energy diagrams of $4e^-$ ORR for H_2O product on TM-NM-GY.

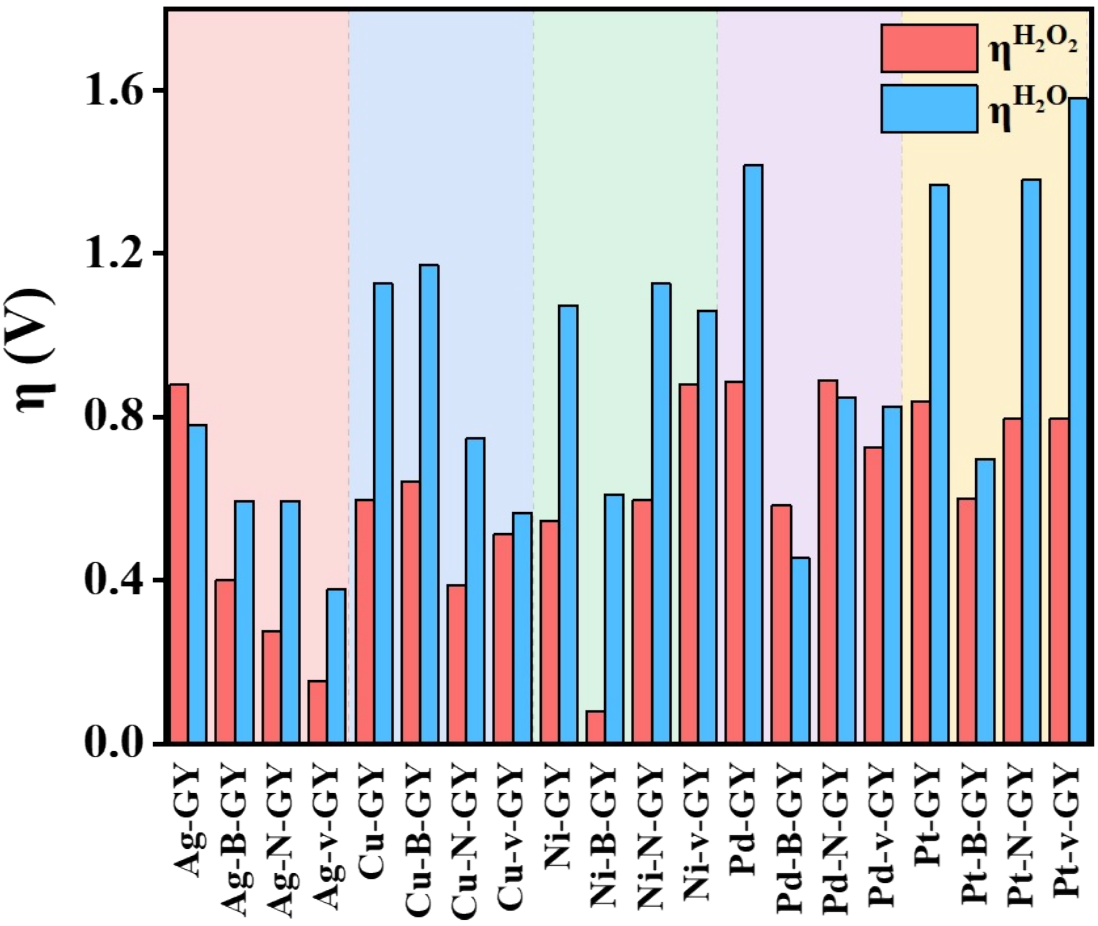

Fig. S12. The selectivity of TM-NM-GY by compare the overpotential of $\eta^{H_2O_2}$ and η^{H_2O}.

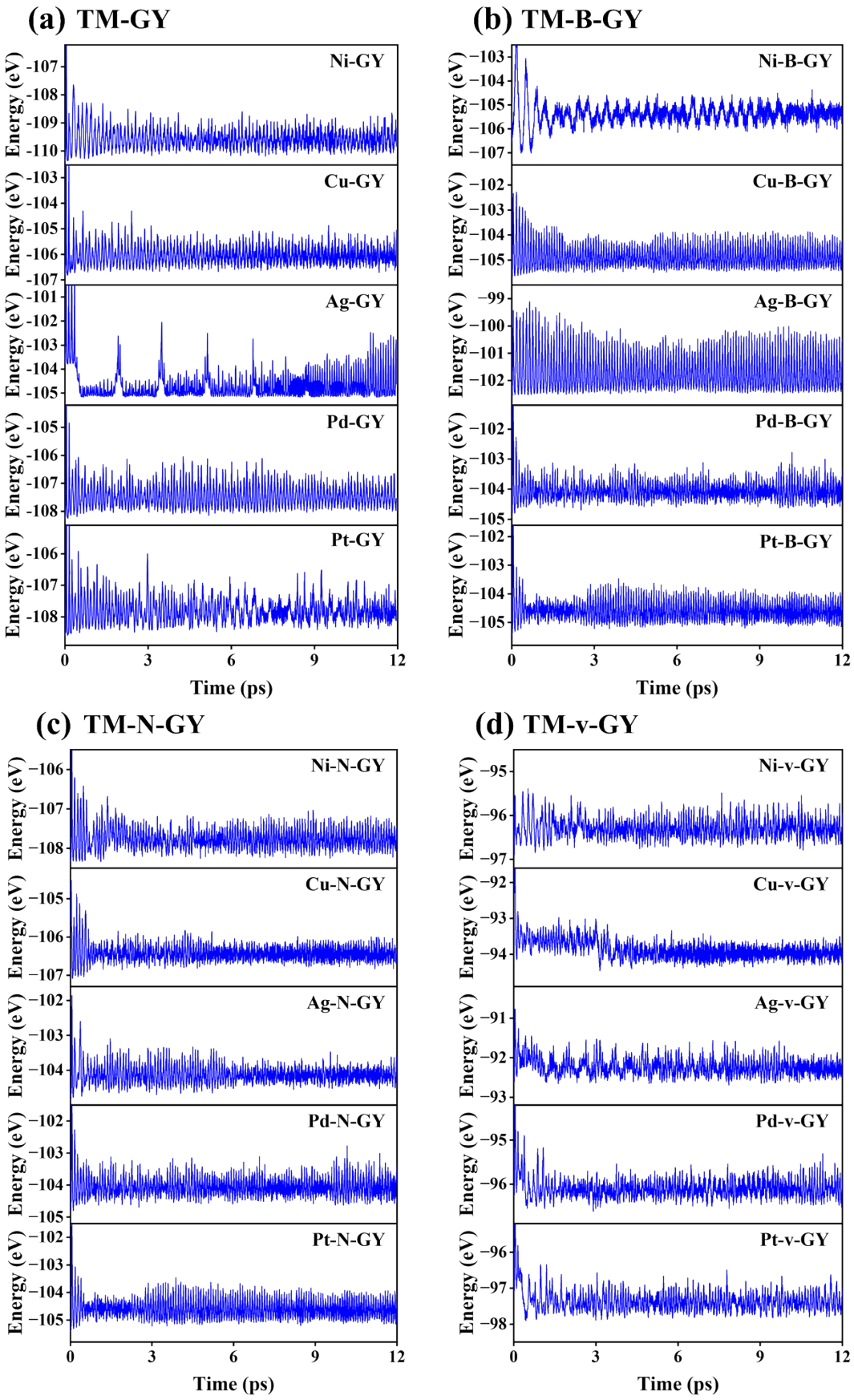

Fig. S13. The AIMD calculation for TM-NM-GY catalysts at 300 K from 0 to 12 ps.

	Energy	AIMD	Electrochemical	Comprehensive stability
Ni-GY	√	√	×	
Cu-GY	×	√	√	
Ag-GY	×	×	×	
Pd-GY	×	√	√	
Pt-GY	×	√	√	
Ni-B-GY	√	√	√	√
Cu-B-GY	√	√	√	√
Ag-B-GY	×	×	√	
Pd-B-GY	×	√	√	
Pt-B-GY	×	√	√	
Ni-N-GY	×	√	×	
Cu-N-GY	×	√	×	
Ag-N-GY	×	×	×	
Pd-N-GY	×	√	√	
Pt-N-GY	×	√	√	
Ni-v-GY	√	√	√	√
Cu-v-GY	√	√	√	√
Ag-v-GY	√	√	√	√
Pd-v-GY	√	√	√	√
Pt-v-GY	√	√	√	√

Fig. S14. Comprehensive evaluation of stability summary for TM-NM-GY.

	Stability	Active (η<0.6V)	Selectivity	All performance
Ni-GY	×	√	√	
Cu-GY	×	√	√	
Ag-GY	×	×	×	
Pd-GY	×	×	√	
Pt-GY	×	×	√	
Ni-B-GY	√	√	√	√
Cu-B-GY	√	×	√	
Ag-B-GY	×	√	√	
Pd-B-GY	×	√	×	
Pt-B-GY	×	√	√	
Ni-N-GY	×	√	√	
Cu-N-GY	×	√	√	
Ag-N-GY	×	√	√	
Pd-N-GY	×	×	×	
Pt-N-GY	×	×	√	
Ni-v-GY	√	×	√	
Cu-v-GY	√	√	√	√
Ag-v-GY	√	√	√	√
Pd-v-GY	√	×	√	
Pt-v-GY	√	×	√	

Fig. S15. Comprehensive evaluation summary of overall catalytic performance through activity, selectivity, and stability for TM-NM-GY.

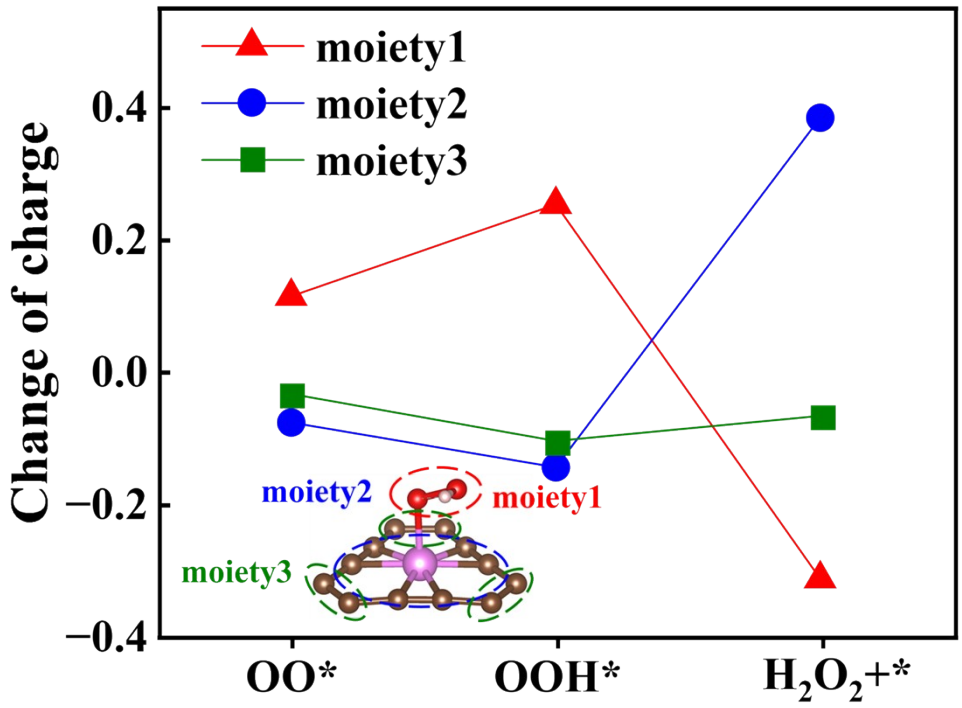

Fig. S16. The charge variation of $2e^-$ ORR reaction for Ni-GY.

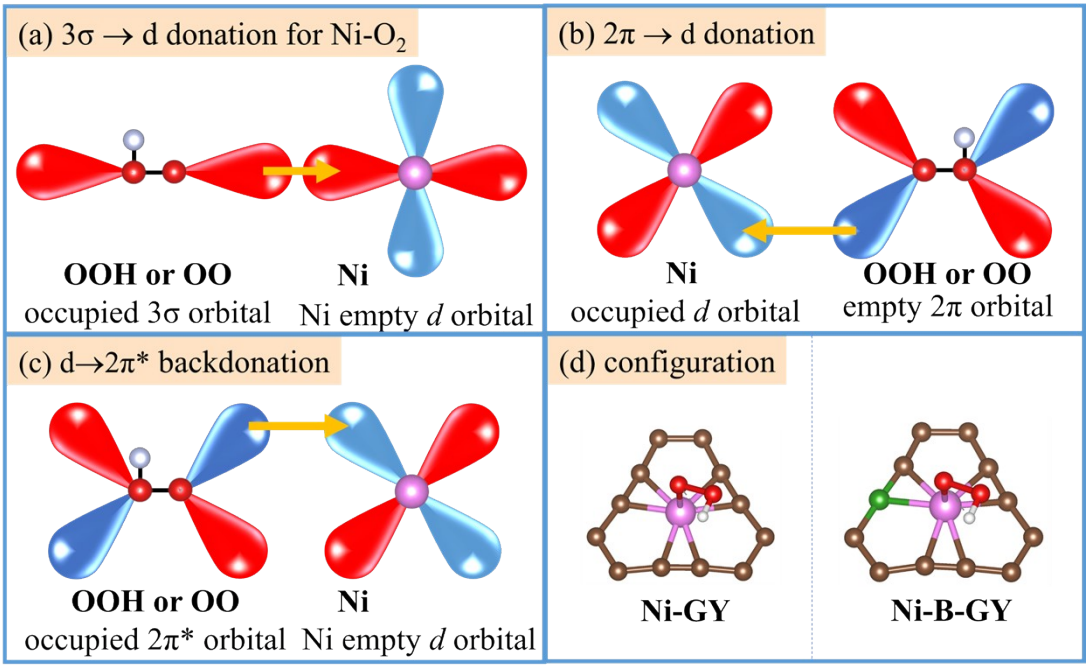

Fig. S17. The donation and back-donation models between Ni and OO or OOH.

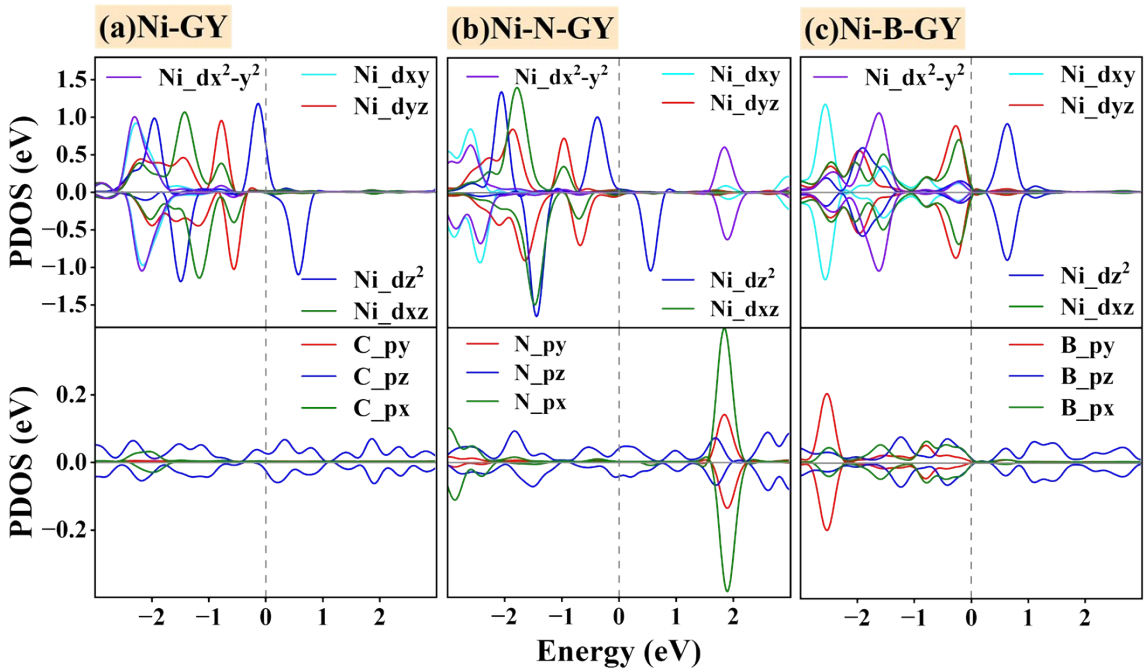

Fig. S18. The PDOS of C, N, B and Ni for Ni-GY, Ni-N-GY and Ni-B-GY.

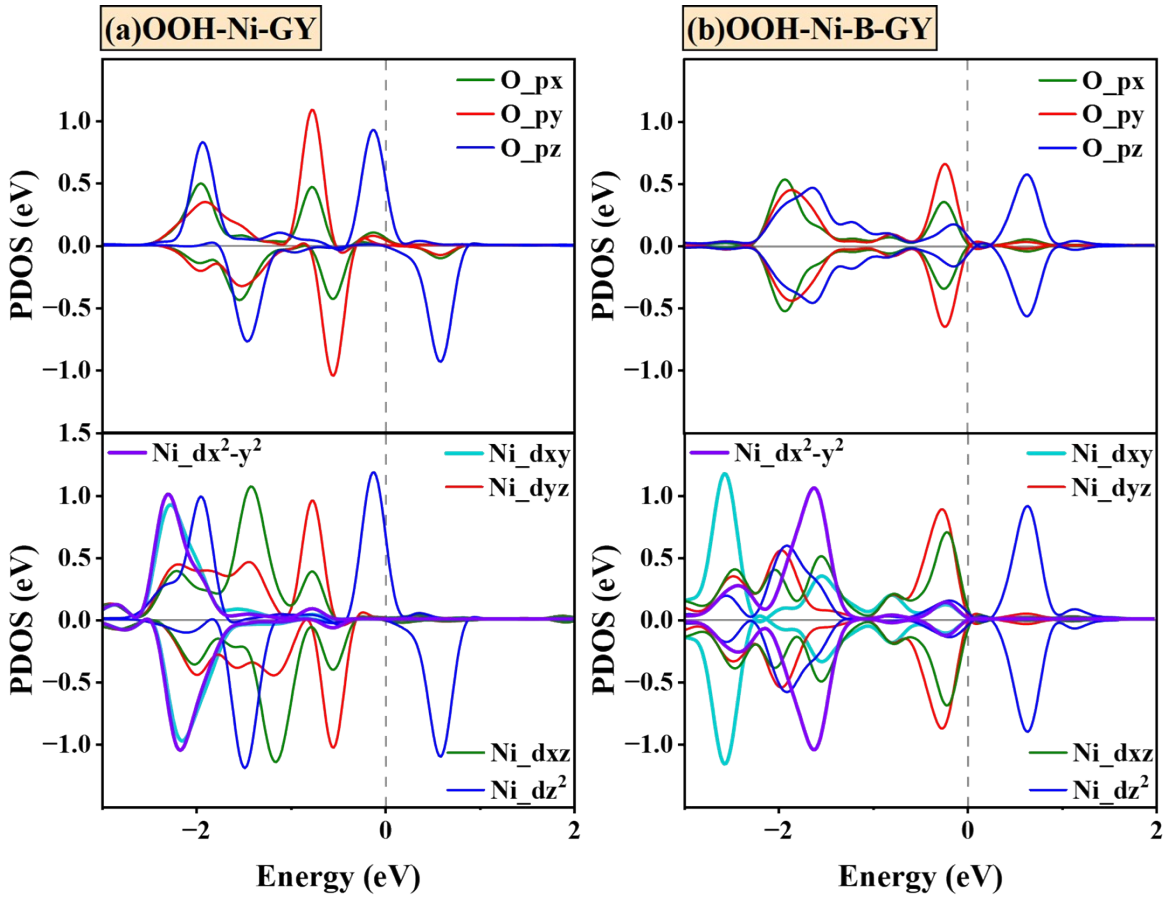

Fig. S19. The PDOS of O (in OOH) and Ni for Ni-GY and Ni-B-GY.

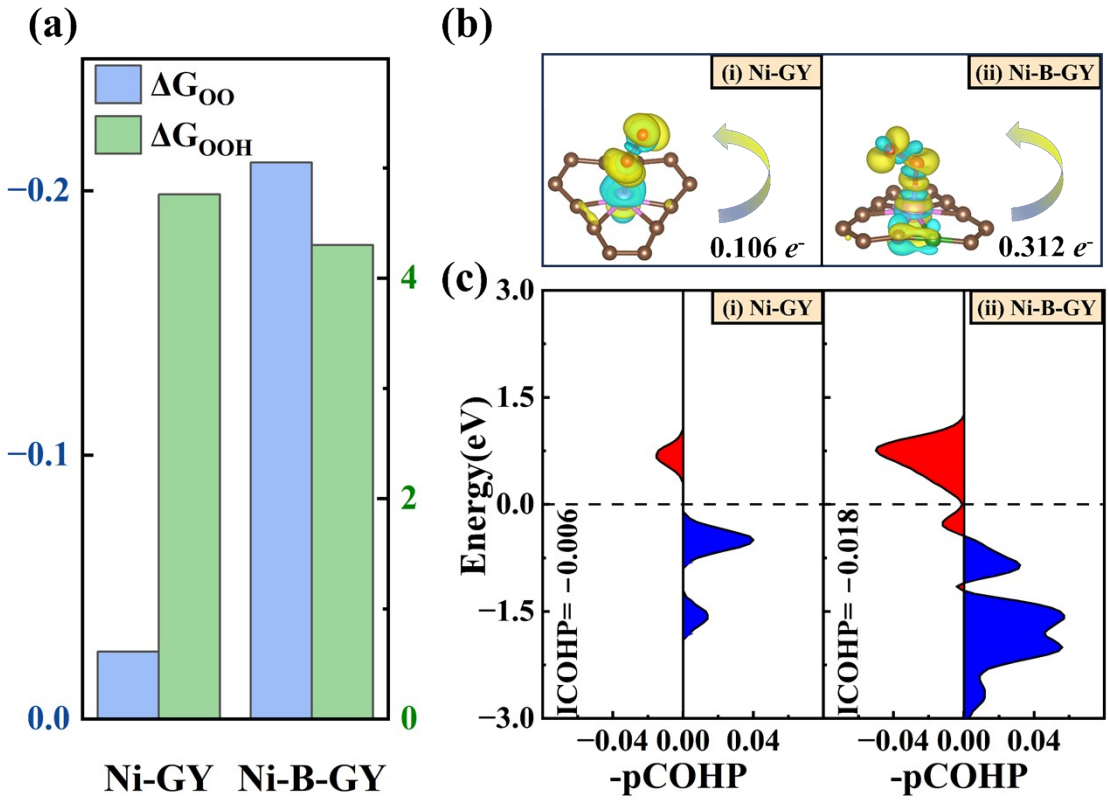

Fig. S20. Ni-GY vs Ni-B-GY: (a) The ΔG_{OO} and ΔG_{OOH}, (b) Charge density difference for OO*, (c) The COHP between the O (in OO*) and Ni.

References

[1] W. Zhang, Y.J. Gao, Q.J. Fang, J.K. Pan, X.C. Zhu, S.W. Deng, Z.H. Yao, G.L. Zhuang, J.G. Wang, High-performance single-atom Ni catalyst loaded graphyne for H_2O_2 green synthesis in aqueous media, J. Colloid Inter. Sci. 599 (2021) 58-67.

[2] G. Di Liberto, L. Giordano, G. Pacchioni, Predicting the stability of single-atom catalysts in electrochemical reactions, ACS Catal. 14(1) (2023) 45-55.

[3] Y. Cao, C. Zhao, Q. Fang, X. Zhong, G. Zhuang, S. Deng, Z. Wei, Z. Yao, J. Wang, Hydrogen peroxide electrochemical synthesis on hybrid double-atom (Pd–Cu) doped N vacancy g-C_3N_4: a novel design strategy for electrocatalyst screening, J. Mater. Chem. A 8(5) (2020) 2672-2683.

[4] J. Liu, Catalysis by supported single metal atoms, ACS Catal. 7 (1) (2016) 34-59.